Molecular control of photoexcited charge transfer and recombination at a quaterthiophene/zinc oxide interface

Weiwei Mou,[1] Satoshi Ohmura,[1,2] Fuyuki Shimojo,[1,2] and Aiichiro Nakano[1]

[1]*Collaboratory for Advanced Computing and Simulations, Department of Physics and Astronomy, Department of Computer Science, Department of Chemical Engineering and Materials Science, University of Southern California, Los Angeles, California 90089-0242, USA*
[2]*Department of Physics, Kumamoto University, Kumamoto 860-8555, Japan*

Nonadiabatic quantum molecular dynamics simulations are performed to study photoexcited charge transfer (CT) and charge recombination (CR) at an interface between a conjugated oligomer donor, quaterthiophene (QT), and an inorganic acceptor (ZnO). Simulations reveal a detrimental effect of *static* disorder in QT conformation on the efficiency of hybrid QT/ZnO solar cells due to increased CR. On the contrary, *dynamic* disorder (i.e., fluctuation of carbon-hydrogen bonds in QT) is essential for high efficiency by assisting CT. The separate controllability of CT and CR at the molecular level has impacts on molecular design for efficient solar cells and explains recent experimental observations. © *2012 American Institute of Physics*. [http://dx.doi.org/10.1063/1.4719206]

Recently, intense research has focused on hybrid solar cells consisting of conjugated polymer, poly(3-hexylthiophene) (P3HT),[1–3] or oligomer, quaterthiophene (QT),[1] as a photoabsorbing and electron-donor material and zinc oxide (ZnO) as an acceptor. In such organic/inorganic systems, organic materials have the advantage of being mechanically flexible and solution processable,[4–6] while inorganic semiconductors are more stable and their band gaps can be engineered.[7,8] However, the major challenge toward addressing the global energy problem[9] is the low power-conversion efficiency of these hybrid systems.[10] Recent experiments combining grazing incidence x-ray diffraction and photocurrent measurements have demonstrated a dramatic increase of photocurrent with improved crystallinity of P3HT at P3HT/ZnO interfaces.[2] This suggests a possibility of interfacial design for improved power-conversion efficiency of hybrid organic/semiconductor solar cells, for which the key is to understand atomistic mechanisms of interfacial charge transfer (CT) of a photoexcited electron from donor to acceptor as well as charge recombination (CR) back to donor.[11] Rapid CT generates photocurrent and is crucial for high efficiency, while CR must be prevented so as not to reduce the current.[12,13] The key question is can we separately control CT and CR by interfacial molecular design?

Here, nonadiabatic quantum molecular dynamics (NAQMD) simulation[14] provides an answer to this question. We study the effect of interfacial structures on CT and CR processes at a QT/ZnO interface using quantum molecular dynamics (QMD) simulations incorporating nonadiabatic electronic transitions[15–20] based on the time-dependent density functional theory (TDDFT) and the fewest-switches surface-hopping (FSSH) approach.[21] Due to the computational limitation, it is common to model P3HT by oligothiophene such as bithiophene,[3] QT, or sexithiophene.[22] Simulation results show increased CR rates due to the twisting of thiophene rings in QT, which explains the experimentally observed correlation between the interfacial P3HT structure and the power-conversion efficiency of hybrid P3HT/ZnO solar cells.[2] We also find that rapid CT from QT to ZnO is

assisted by the fluctuation of the C–H bond length in QT around its equilibrium value. Our QMD simulations thus provide insights into better molecular design of thiophene/ZnO interfaces for efficient solar cells. Namely, *static* disorder of the thiophene conformation at the interface is detrimental due to increased CR rates, whereas *dynamic* disorder is essential for high efficiency by enhancing CT rates. Thus, CT and CR can be separately controlled by molecular design.

The simulated system is shown in Fig. 1. A slab of ZnO with dimensions $28.07 \times 15.56 \times 12.97 \text{ Å}^3$ (containing 240 O and 240 Zn atoms) is cut out from bulk wurtzite crystal of experimental lattice constants, $a = 3.2417 \text{ Å}$ and $c = 5.1876 \text{ Å}$.[23,24] A large vacuum layer of thickness ~8 Å is added in the z direction, thereby exposing two $(10\bar{1}0)$ surfaces labeled γ and δ in Fig. 1(b). Periodic boundary conditions are applied to all Cartesian directions for the resulting simulation supercell of dimensions $28.07 \times 15.56 \times 21 \text{ Å}^3$.[25] The ZnO slab is relaxed to the minimum-energy configuration using the conjugate-gradient method, where the interatomic forces are calculated quantum mechanically in the framework of density functional theory (DFT).[14] The surface consists of Zn-O dimer rows in the $[1\bar{2}10]$ direction, forming trenches in between. A QT molecule (CH_3-$(C_{14}H_{16}S_2)_2$-CH_3 consisting of 4 thiophene rings) is placed on top of a trench along the $[1\bar{2}10]$ direction, which was found to be the minimum-energy interfacial structure based on an *ab initio* calculation,[3,22] making the total QT/ZnO system to contain 552 atoms. The distance between the thiophene-rings plane (labeled α in Fig. 1(b)) and the dimerized ZnO surface (labeled γ) is set as 3.1 Å, which gives the minimum energy over different distances. The distance of ~5 Å between the QT and the neighboring ZnO δ surface in the periodic image causes negligible interaction between them. Namely, a larger supercell of $28.07 \times 15.56 \times 23 \text{ Å}^3$ only slightly changes the total energy (by ~0.01 meV/atom).

We first calculate the alignment of electronic energy levels in our QT/ZnO system based on DFT. The energy levels of the initial configuration are shown in the left panel of Fig. 2(b), which shows partial electronic densities of states
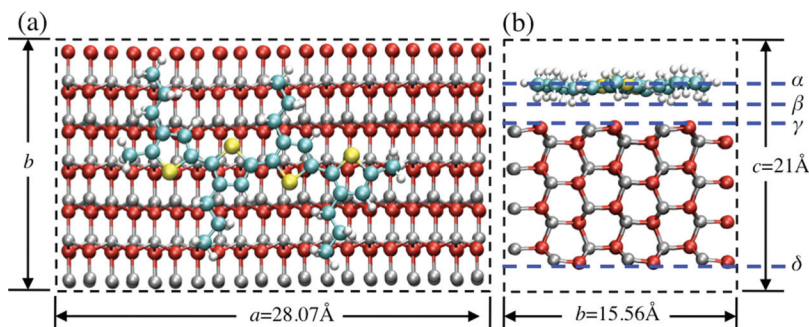
FIG. 1. (a) Top view and (b) side view of the simulated QT molecule on a ZnO $(10\bar{1}0)$ surface, where the red, gray, cyan, yellow, and white spheres represent O, Zn, C, S, and H atoms, respectively. The blue dashed lines indicate planes α, β, γ, and δ discussed in the text.

(DOS) $D_\alpha(E)$ projected onto the wave functions of the atoms in the α-th molecular subsystems ($\alpha = $ ZnO or QT), where the energy is measured relative to the Fermi energy. The highest occupied molecular orbital (HOMO) at -0.95 eV spreads only within QT, reflected in a peak of $D_{QT}(E)$ in Fig. 2(b), and its wave function shown in Fig. 2(a) is nearly identical to the HOMO of isolated QT. On the other hand, the lowest unoccupied molecular orbital (LUMO) at 1.04 eV resides only within ZnO as shown in Fig. 2(a) and the corresponding peak in $D_{ZnO}(E)$ in Fig. 2(b). The lowest unoccupied orbitals with significant wave-function amplitudes within QT are LUMO+3 (1.67 eV) and LUMO+4 (1.93 eV), of which the LUMO+4 state has the largest amplitude in QT and thus represents the LUMO of QT or LUMO(QT). Here, we denote the m-th lowest unoccupied orbital but one as LUMO+m, and the wave functions of LUMO+3 and LUMO+4 are shown in Fig. 2(a). The highest occupied molecular orbital but two (i.e., HOMO−2) at -2.11 eV is a ZnO state with no mixture of QT orbitals. We therefore call HOMO−2 to be the HOMO of ZnO or HOMO(ZnO). The DFT calculation correctly describes the known band alignment: HOMO(QT) falls within the band gap of ZnO, and LUMO(QT) falls in the conduction band of ZnO. Accordingly, the simulations described below entail the correct physics of experimental QT/ZnO systems, i.e., photo-excitation occurs at the electron donor side by exciting an electron from HOMO(QT) to LUMO(QT), followed by CT of the photo-excited electron from LUMO(QT) to the conduction band of ZnO, leaving a hole in HOMO(QT), with potential CR from LUMO(ZnO) back to HOMO(QT). The calculated energy gap between HOMO(QT) and LUMO(QT) is 2.88 eV, which agrees reasonably with the observed value of 3.16 eV for QT.[26] Also, the calculated energy gap between HOMO(ZnO) and LUMO(ZnO) is 3.15 eV, which also agrees with the experimental value of 3.4 eV.[27] The alignment among the levels relevant for CT and CR processes—HOMO(QT), LUMO(QT), and LUMO(ZnO)—is correctly described by the present calculation.

Next, we study how the band alignment is affected by molecular motions. An adiabatic QMD simulation is performed at a temperature of $T = 300$ K in the canonical ensemble.[28–30] The right panel of Fig. 2(b) shows the time evolution of electronic eigenenergies ε_i, in which the HOMO(QT), LUMO(QT), HOMO(ZnO), and LUMO(ZnO) levels are labeled. Here, the partial DOS analysis is performed at each MD step to characterize the states. While HOMO(QT) is a pure QT state and HOMO(ZnO) is a pure ZnO state, LUMO(QT) is a highly coupled state with both $D_{QT}(E)$ and $D_{ZnO}(E)$ peaks at the corresponding energy and LUMO(ZnO) also has a small mixture of QT orbitals. The identification of these four states is consistent with the wave functions in Fig. 2(a).

The fluctuation of $\varepsilon_i(t)$ in Fig. 2(b) within the time scale of 20 fs does not drastically change the band alignment. To study molecular mechanisms to alter the alignment, we perform adiabatic QMD simulation for a longer time. The alignment of energy levels can be characterized by energy gaps: $\Delta E_{CR} = \varepsilon_{LUMO(ZnO)} - \varepsilon_{HOMO(QT)}$, which is relevant for CR, and $\Delta E_{CT} = \varepsilon_{LUMO(QT)} - \varepsilon_{LUMO(ZnO)}$; see Fig. 3(a). Figure 3(c) plots ΔE_{CT} (red line) and ΔE_{CR} (blue line) versus time in the range of 0–1200 fs, together with the time evolution of the deviation $\Delta\Theta$ (black line) of the dihedral angle Θ between thiophene rings in QT (as defined in Fig. 3(b)) from its equilibrium value. The $\Delta\Theta$ in Fig. 3(c) is the averaged value over all three inter-ring dihedral angles. The vertical dashed gray lines mark typical maxima and minima labeled A∼I. In particular, $\Delta\Theta(t)$ and $\Delta E_{CT}(t)$ exhibit coincidental
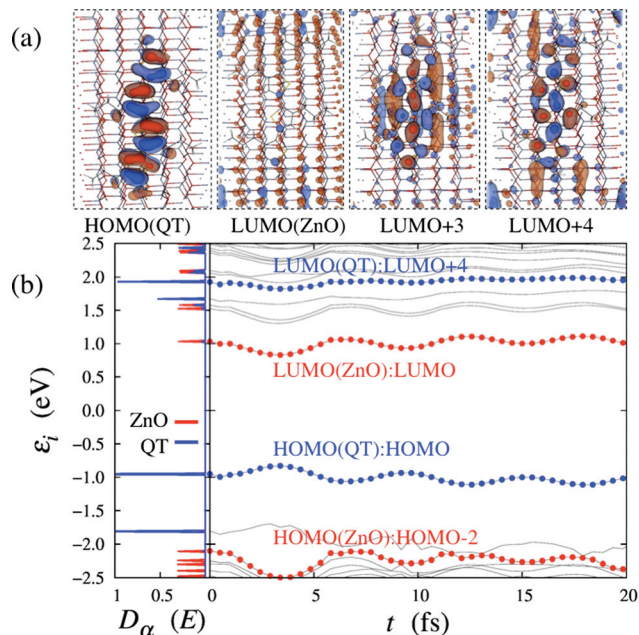

FIG. 2. (a) Spatial distribution of electronic wave functions in the ground state, for HOMO, LUMO, LUMO+3, and LUMO+4, where the red and blue isosurfaces correspond to the values of 0.03 and −0.03 a.u., respectively. (b) Electronic densities of states $D_\alpha(E)$ for the initial configuration (left panel), where the red and blue curves are, respectively, for $\alpha = $ ZnO and QT. The right panel shows the time evolution of electronic eigenenergies during adiabatic QMD simulation. The blue curves indicate LUMO(QT) and HOMO(QT), whereas the red curves are LUMO(ZnO) and HOMO(ZnO).
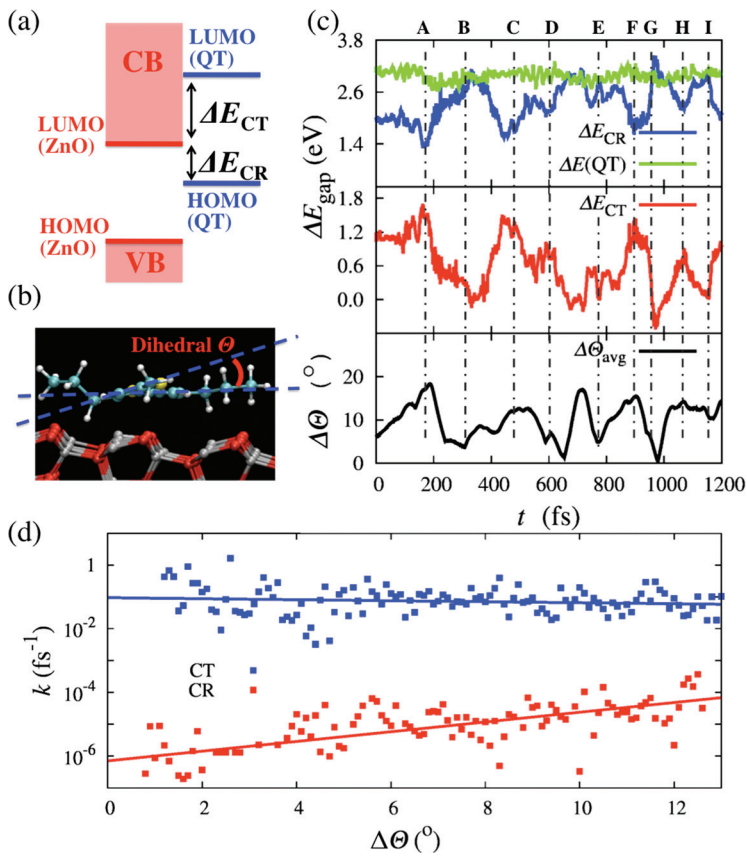
FIG. 3. (a) Schematic of the alignment of electronic energy levels of QT/ZnO, where CB and VB denote the conduction band and valence band of ZnO. (b) The inter-ring dihedral angel Θ, where the red, gray, cyan, yellow, and white spheres represent O, Zn, C, S, and H atoms, respectively, in the side view of the QT/ZnO interface. (c) Time evolution of the deviation $\Delta\Theta$ of the dihedral angle from its equilibrium value (bottom panel), energy gap ΔE_{CT} (middle panel), and energy gaps ΔE_{CR} and $\Delta E(QT) = \varepsilon_{LUMO(QT)} - \varepsilon_{HOMO(QT)}$ (top panel). (d) CT (blue) and CR (red) rates versus $\Delta\Theta$. The lines are the least-square fits.

maxima at A, C, D, F, and H, while $\Delta E_{CR}(t)$ has minima at the corresponding times. Similarly, $\Delta\Theta(t)$ and $\Delta E_{CT}(t)$ show coincidental minima, whereas $\Delta E_{CR}(t)$ shows maxima, at B, E, G, and I. Pearson's correlation coefficients corr(ΔE_{CT}, $\Delta\Theta$) and corr(ΔE_{CR}, $\Delta\Theta$) are 0.53 and −0.51, respectively, demonstrating that ΔE_{CT} is positively correlated with the deviation $\Delta\Theta$ of the inter-ring dihedral angle, while ΔE_{CR} is negatively correlated with $\Delta\Theta$. The sum of ΔE_{CT} and ΔE_{CR} is the band gap of QT, i.e., $\Delta E(QT) = \Delta E_{CT} + \Delta E_{CR} = \varepsilon_{LUMO(QT)} - \varepsilon_{HOMO(QT)}$, and the green curve in Fig. 3(c) shows its time evolution. $\Delta E(QT)$ fluctuates around an average value of 2.97 eV with its larger values corresponding to larger $\Delta\Theta$ (see Fig. S2 in Ref. 14). This is consistent with previous theoretical[31] and experimental[32] observations on P3HT that reduced regioregularity (hence larger Θ) leads to larger band gap (note that the equilibrium Θ is 0 in our case).

To study the effects of ΔE_{CR} on nonadiabatic electronic transitions, we numerically solve TDDFT equations,[15–20,33,34] starting from various configurations in the adiabatic QMD trajectory in Fig. 3(c). Starting from each configuration, TDDFT equations are solved with the adiabatic Kohn-Sham (KS) basis in DFT. From the density-matrix elements, we calculate the transition probability $\gamma_{ij}(t)$ from the current adiabatic state i to another, j, as a function of time. The nuclei are treated classically in the adiabatic representation, i.e., the atomic forces are calculated from the (excited) electronic eigenstates for the current nuclear positions. The CT and CR rates are then estimated as $k_{CT} = \gamma_{LUMO(QT),j}(t)/t$ (j is the nearest unoccupied ZnO state to LUMO(QT)) and $k_{CR} = \gamma_{LUMO(ZnO),HOMO(QT)}(t)/t$, respectively. Figure 3(d) plots k_{CT} and k_{CR} as a function of $\Delta\Theta$,

where each symbol represents an average rate over tens to hundreds configurations with the same value of $\Delta\Theta$. We find that k_{CR} increases by two orders of magnitude when $\Delta\Theta$ increases from 1 to 12°. On the other hand, k_{CT} has no significant correlation with $\Delta\Theta$. Thus, the CR rate significantly increases with the twisting of thiophene rings, while the CT rate is insensitive to it. This is understandable since the CR rate is inversely proportional to ΔE_{CR} according to the time-dependent perturbation theory,[35] where the latter has negative correlation with $\Delta\Theta$ as shown before. On the other hand, the LUMO(QT) level involved in CT is located within the densely populated conduction band of ZnO and its wave function is highly hybridized with ZnO orbitals, and thus the shift of $\varepsilon_{LUMO(QT)}$ due to thiophene-ring twisting has little effect on the CT rate.

It should be noted that such conformational disorder is quenched to produce static defects in hybrid solar cells composed of solid thiophene and ZnO. The above simulation result indicates that such static disorder is detrimental to the solar-cell efficiency by increasing CR and thus reducing the generated photocurrent. Recently, it has been shown experimentally that higher crystallinity of P3HT at the P3HT/ZnO interface can be achieved by adding a self-assembled monolayer (SAM) on the ZnO surface before depositing P3HT and that the improved structural order at the interface increases the photocurrent of P3HT/ZnO solar cells.[2] Our simulation provides an atomistic-level explanation for this phenomenon due to the reduction of the CR rate, while keeping the CT rate constant.

In order to study how a photoexcited electron transfers from QT to ZnO, we perform NAQMD simulation[14] based on the FSSH method[21] together with the KS representation

of Casida's linear-response TDDFT.[15–20,33,34] Nonadiabatic transitions between electronic excited states are accepted stochastically according to the transition probability. The CT excitation energy calculated using the generalized gradient approximation is within 20% from that calculated with a range-separated hybrid exchange-correlation functional[36] (see Fig. S3 in Ref. 14).

Each NAQMD simulation starts with an electronic excited state that corresponds to the excitation of an electron from HOMO(QT) to LUMO(QT) for a given configuration sampled from adiabatic MD trajectory. We calculate the distribution of oscillator strengths using linear-response TDDFT,[37] which confirms that the photoexcitation from HOMO(QT) to LUMO(QT) corresponds to the first photoabsorption peak (see Fig. S4 in Ref. 14). An example of the time evolution of the electronic excitation energies is shown in Fig. 4(b) along with the exciton charge density at selected times in Fig. 4(a). Immediately after the excitation, the quasi-electron charge density has a dominant distribution within the QT molecule; see panel A in Fig. 4(a). The fluctuation drives LUMO(QT) towards ZnO, resulting in the quasi-electron charge density labeled B in Fig. 4(a), which has significant amplitudes in ZnO. Eventually, the quasi-electron charge density evolves to a state labeled C in Fig. 4(a), which has a large overlap with a pure ZnO state labeled D in Fig. 4(a). The large overlap between wave functions constituting excited electronic states, along with the approaching/crossing of the excitation energies, results in a large transition probability from C to D; see Fig. 4(b). The transition results in a stable pure ZnO state (see label D in Fig. 4(a)) to complete CT from QT to ZnO. This CT is assisted by the crossing of excitation energies, which in turn is caused by a characteristic oscillation of the electronic excitation energies with a period of 5.8 fs, e.g., between the

time 55–60 fs in Fig. 4(b). We have found that this oscillation is caused by the fluctuation of the C–H bond length in QT around its equilibrium value. Namely, the excitation-energy oscillation has exactly the same frequency as that of $\delta l(t) = |l_{CH}(t) - l_{avg}|$, where $l_{CH}(t)$ is the average length of all C–H bonds on the thiophene pentagon rings and l_{avg} is its time average (see Fig. S5 in Ref. 14). This mechanism also explains the experimentally observed efficiency enhancement by the insertion of a SAM at P3HT/ZnO interfaces.[2] We have performed additional simulations, in which a SAM inserted at the donor/acceptor interface is shown to weaken the bonding between the donor and acceptor layers, thereby liberating C–H vibrations in interfacial thiophene rings to better assist CT (see Fig. S6 in Ref. 14).

In order to estimate the CT rate, we integrate the quasi-electron charge density at the QT side above the β plane shown in Fig. 1(b) to obtain the probability R_{QT}. Similarly, we calculate R_{ZnO} below the β plane (note that $R_{ZnO} + R_{QT} = 1$) during the entire electron-transfer process up to ~100 fs. Figure 4(c) plots an ensemble average over 50 such NAQMD simulations starting from 50 configurations uniformly sampled from the adiabatic MD trajectory shown in Fig. 3(c). Though CT occurs at different times on different trajectories, all transitions are assisted by the oscillation of excitation energies of the same period of 5.8 fs. The averaged $R_\alpha(t)$ indicates that rapid CT completes within 70 fs. The corresponding CT rate is 0.014 fs^{-1}.

In summary, charge transfer and recombination at QT/ZnO interface have been studied by quantum molecular dynamics simulations. It is found that the inter-ring dihedral angles in QT controls the band alignment, which provides an atomistic explanation on why P3HT with better ordering on ZnO inhibits CR, leading to higher solar cell efficiency. Nonadiabatic QMD simulations show that CT is assisted by the fluctuation of the C–H bond length on the thiophene pentagon rings of QT around its equilibrium value. The molecular mechanisms found here provide some insights on the interfacial electron transfer and recombination. Namely, the alignment between the donor and acceptor energy bands and accordingly the CR rate can be controlled through static molecular conformations at the donor/acceptor interface, whereas the CT rate can be enhanced by molecular design allowing sufficient bond-stretching motions.
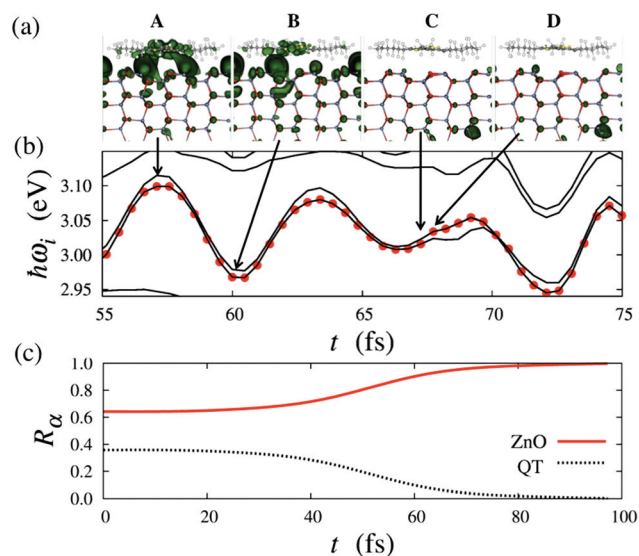
FIG. 4. (a) Spatial distribution of the exciton charge density at different time steps A, B, C, and D, where isosurfaces of the quasi-electron charge density of 0.02 a.u. is shown in green. (b) Time evolution of electronic excitation energies during 55–75 fs in NAQMD simulation. The occupied excited state is indicated by red solid circles. (c) Averaged time evolution of the existence probabilities $R_\alpha(t)$ of the pseudo-electron in subsystems α. The red and black lines indicate $\alpha =$ ZnO and QT, respectively.

[1]A. L. Briseno, T. W. Holcombe, A. I. Boukai, E. C. Garnett, S. W. Shelton, J. J. M. Frechet, and P. D. Yang, Nano Lett. **10**(1), 334–340 (2010).
[2]J. W. P. Hsu and M. T. Lloyd, MRS Bull. **35**(6), 422–428 (2010).
[3]S. Dag and L. W. Wang, Nano Lett. **8**(12), 4185–4190 (2008).

[4]G. Dennler, M. C. Scharber, and C. J. Brabec, Adv. Mater. **21**(13), 1323–1338 (2009).

[5]H. Sirringhaus, T. Kawase, R. H. Friend, T. Shimoda, M. Inbasekaran, W. Wu, and E. P. Woo, Science **290**(5499), 2123–2126 (2000).

[6]S. R. Forrest, Nature (London) **428**(6986), 911–918 (2004).

[7]C. Y. Li, T. C. Wen, T. H. Lee, T. F. Guo, J. C. A. Huang, Y. C. Lin, and Y. J. Hsu, J. Mater. Chem. **19**(11), 1643–1647 (2009).

[8]D. C. Olson, S. E. Shaheen, M. S. White, W. J. Mitchell, M. F. A. M. van Hest, R. T. Collins, and D. S. Ginley, Adv. Funct. Mater. **17**(2), 264–269 (2007).

[9]G. W. Crabtree and N. S. Lewis, Phys. Today **60**(3), 37–42 (2007).

[10]S. D. Oosterhout, M. M. Wienk, S. S. van Bavel, R. Thiedmann, L. J. A. Koster, J. Gilot, J. Loos, V. Schmidt, and R. A. J. Janssen, Nat. Mater. **8**(10), 818–824 (2009).

[11]Y. Y. Lin, Y. Y. Lee, L. W. Chang, J. J. Wu, and C. W. Chen, Appl. Phys. Lett. **94**(6), 063308 (2009).

[12]N. C. Giebink, G. P. Wiederrecht, M. R. Wasielewski, and S. R. Forrest, Phys. Rev. B **82**(15), 155305 (2010).

[13]Y. Fu, Y. H. Zhou, H. B. Su, F. Y. C. Boey, and H. Agren, J. Phys. Chem. C **114**(9), 3743–3747 (2010).

[14]See supplementary material http://dx.doi.org/10.1063/1.4719206 for simulation details.

[15]N. L. Doltsinis and D. Marx, Phys. Rev. Lett. **88**(16), 166402 (2002).

[16]C. F. Craig, W. R. Duncan, and O. V. Prezhdo, Phys. Rev. Lett. **95**(16), 163001 (2005).

[17]E. Tapavicza, I. Tavernelli, and U. Rothlisberger, Phys. Rev. Lett. **98**(2), 023001 (2007).

[18]C. P. Hu, O. Sugino, H. Hirai, and Y. Tateyama, Phys. Rev. A **82**(6), 062508 (2010).

[19]S. Ohmura, S. Koga, I. Akai, F. Shimojo, R. K. Kalia, A. Nakano, and P. Vashishta, Appl. Phys. Lett. **98**(11), 113302 (2011).

[20]X. Zhang, Z. Li, and G. Lu, Phys. Rev. B **84**(23), 235208 (2011).

[21]J. C. Tully, J. Chem. Phys. **93**(2), 1061–1071 (1990).

[22]N. Sai, K. Leung, and J. R. Chelikowsky, Phys. Rev. B **83**(12), 121309 (2011).

[23]D. A. Fletcher, R. F. McMeeking, and D. Parkin, J. Chem. Inf. Comput. Sci. **36**(4), 746–749 (1996).

[24]S. Ito, T. Shimazaki, M. Kubo, H. Koinuma, and S. Sumiya, J. Chem. Phys. **135**(24), 241103 (2011).

[25]See Fig. S1 in Ref. 14 for a dipole correction to the periodic boundary condition.

[26]T. Izumi, S. Kobashi, K. Takimiya, Y. Aso, and T. Otsubo, J. Am. Chem. Soc. **125**(18), 5286–5287 (2003).

[27]P. Ravirajan, A. M. Peiro, M. K. Nazeeruddin, M. Graetzel, D. D. C. Bradley, J. R. Durrant, and J. Nelson, J. Phys. Chem. B **110**(15), 7635–7639 (2006).

[28]S. Nose, Mol. Phys. **52**(2), 255–268 (1984).

[29]W. G. Hoover, Phys. Rev. A **31**(3), 1695–1697 (1985).

[30]F. Shimojo, S. Ohmura, R. K. Kalia, A. Nakano, and P. Vashishta, Phys. Rev. Lett. **104**(12), 126102 (2010).

[31]D. P. McMahon, D. L. Cheung, L. Goris, J. Dacuna, A. Salleo, and A. Troisi, J. Phys. Chem. C **115**(39), 19386–19393 (2011).

[32]G. Dicker, T. J. Savenije, B. H. Huisman, D. M. de Leeuw, M. P. de Haas, and J. M. Warman, Synth. Met. **137**(1–3), 863–864 (2003).

[33]S. Meng and E. Kaxiras, J. Chem. Phys. **129**(5), 054110 (2008).

[34]I. Vasiliev, S. Ogut, and J. R. Chelikowsky, Phys. Rev. Lett. **82**(9), 1919–1922 (1999).

[35]J. M. An, M. Califano, A. Franceschetti, and A. Zunger, J. Chem. Phys. **128**, 164720 (2008).

[36]Y. Tawada, T. Tsuneda, S. Yanagisawa, T. Yanai, and K. Hirao, J. Chem. Phys. **120**(18), 8425–8433 (2004).

[37]M. E. Casida, in *Recent Advances in Density Functional Methods*, Part I, edited by D. P. Chong (World Scientific, Singapore, 1995), pp. 155–192.